Annals of Nuclear Energy 59 (2013) 126–138

Contents lists available at SciVerse ScienceDirect

Annals of Nuclear Energy

journal homepage: www.elsevier.com/locate/anucene

The experimental determination and evaluation of the spectral indices of the IPEN/MB-01 reactor for the IRPhE project

Adimir dos Santos *, Leda C.C.B. Fanaro, Rogério Jerez

Instituto de Pesquisas Energéticas e Nucleares (IPEN-CNEN/SP), Centro de Engenharia Nuclear (CEN), Av. Prof. Lineu Prestes, 2242, Cidade Universitária, 05508-000 São Paulo, SP, Brazil

ARTICLE INFO

Article history:
Received 23 January 2013
Accepted 29 March 2013
Available online 30 April 2013

Keywords:
Spectral indices
Benchmarks
IPEN/MB-01 reactor
$^{28}\rho^*$
$^{25}\delta^*$

ABSTRACT

New experimental results for the spectral indices of the IPEN/MB-01 reactor are presented in this work. The experimental approach considers a new technique for the $^{28}\rho$ case which does not require any sort of calculated correction factors. This aspect gave to the IPEN/MB-01 experiment an excellent quality and free of possible bias due to these calculated correction factors. The uncertainty analysis show, even considering the uncertainties of the geometric and material data of the facility, that the final uncertainties are small enough and well understood for a benchmark problem. The experiment was evaluated and included in the IRPhE handbook. The theory/experiment comparison reveals that there is considerable progress in the ^{238}U nuclear data for application in thermal reactors. The theory/experiment comparison employs the nuclear data libraries ENDF/B-VII.0, ENDF/B-VI.8, JEF3.1, and JENDL3.3 and reveals an excellent agreement for the spectral index $^{28}\rho^*$ independently of the nuclear data library considered; aspect never found before in several other comparisons. The long term overprediction of the ^{238}U neutron epithermal capture appears to be eliminated with the improvements in the recent nuclear data libraries. The experimental performed at the IPEN/MB-01 reactor supports the changes in the ^{238}U nuclear data incorporated in ENDF/B-VII.0 as well as in the other libraries studied in this work. The theory/experiment comparison of $^{25}\delta^*$ and $(C8/F)_{ept}$ show that these spectral indices are in general slightly overpredicted, thus suggesting that the thermal fission cross section of ^{235}U might be a little bit underestimated. The overall analysis of the theory/experiment comparisons show the excellent applicability of ENDF/B-VII.0 for thermal reactors fuelled with slightly enriched uranium.

1. Introduction

Experiments involving determination of the reaction rates in the fuel pellets are of fundamental importance to correlate theory and experiment mainly concerning mathematical methods and related nuclear data libraries. These experiments are normally performed through the irradiation of bare and Cadmium covered fertile and/or fissile foils. Typical examples are the spectral indices $^{28}\rho$ and $^{25}\delta$ which provide the ratio of the epithermal to thermal neutron captures in ^{238}U and the ratio of the epithermal to thermal fission in ^{235}U respectively. Highly enriched foils are used for the measurements of $^{25}\delta$ and depleted uranium foils are used for $^{28}\rho$. The method basically consists in the determination of the Cadmium ratio and the transformation of the perturbed system into a non-perturbed by means of calculated correction factors (Bitelli, 2001; Sher and Fiarman, 1976). Furthermore, the corrections are also applied to transform the thermal cutoff to 0.625 eV (Sher and Fiarman, 1976). Two major problems occur in the measurements of these spectral indices. The first is the maintenance of same reactor power in the irradiation of the bare and Cadmium covered foils. Usually they are performed in two distinct irradiations. The second problem refers to the introduction of the calculated correction factors. Their uncertainties and the validation of the applied calculation methods are extremely complex and do not have any experimental support for that. The most famous spectral indices measurements for thermal reactor applications are the ones performed in the TRX and BAPL critical facilities selected by the Cross Section Evaluation Working Group (CSEWG, 1974) as benchmarks.

Table 1 (Yudkevich et al., 1994) shows the status of art related to the spectral indices. It can be noted that the discrepancies between theory and experiment are as high as 25% for the NORA reactor. Currently the level of discrepancy runs from −2.0% to +3.0% for the critical facilities TRX (Rahman et al., 2004), BAPL (Rahman et al., 2004), MISTRAL (Courcelle et al., 2006), and ERASME (Courcelle et al., 2006). However, the experimental uncertainties are over 1.5% which makes difficult the comparison between theory and experiment. Besides that, the reported

* Corresponding author. Tel.: +55 11 31339479; fax: +55 11 3133 9423.
E-mail addresses: asantos@ipen.br (A. dos Santos), lcfanaro@ipen.br (L.C.C.B. Fanaro), rjerez@ipen.br (R. Jerez).

0306-4549/$ - see front matter
http://dx.doi.org/10.1016/j.anucene.2013.03.049

Table 1
Comparison between calculated and measured spectral indices.

Experiment	Spectral index	$(C-E)/E$ (%)	Experimental uncertainty (%)
NORA	$^{28}\rho$	+3.0	±1.0
	$^{25}\delta$	+25.0	±0.7
BAY	$^{28}\rho$	+5.0	±0.4
	$^{25}\delta$	−9.0	±6.6
CRX	$^{28}\rho$	+15.0	–
TRX-1[a]	$^{28}\rho$	+3.2	±1.6
	$^{25}\delta$	−0.5	±1.0
TRX-2[a]	$^{28}\rho$	+1.9	±1.9
	$^{25}\delta$	−1.6	±1.3
BAPL-1[a]	$^{28}\rho$	−0.6	±0.7
	$^{25}\delta$	−1.5	±2.4
BAPL-2[a]	$^{28}\rho$	+2.8	±0.9
	$^{25}\delta$	−0.7	±1.5
BAPL-3[a]	$^{28}\rho$	−0.03	±1.1
	$^{25}\delta$	−0.2	±1.9
Mistral-1 (UO_2)[b]	C^{U238}/F^{tot}	+2.2	±2.0
Mistral-2 (UO_2–PuO_2)[b]	C^{U238}/F^{tot}	+2.3	±1.5
Erasme-S (UO_2–PuO_2)[b]	$\sigma_c^{U238}/\sigma_f^{U235}$	+1.6	±2.3
Erasme-R (UO_2–PuO_2)[b]	$\sigma_c^{U238}/\sigma_f^{U235}$	−0.2	±2.1

[a] ENDF/B-VI.
[b] JEFF2.2.

uncertainties do not take into consideration the uncertainties due to the geometric and material data of the facility. A clear aspect seen in Table 1 is that the spectral index $^{28}\rho$ is systematically overpredicted in practically all experiments reported. This overprediction in the spectral index $^{28}\rho$ has been historically mostly credited to the overprediction of the epithermal cross section of ^{238}U. A direct consequence of this effect observed in several facilities was the underprediction of k_{eff} in several critical experiments.

The purpose of this work is to show the experimental determination and evaluation of several spectral indices of the core of the IPEN/MB-01 reactor. The spectral indices considered in this work are the ones based on the ratio of epithermal to thermal reaction rates and on the ratio of specific reaction rates. The first category will consider the very classical spectral indices $^{28}\rho$ and $^{25}\delta$. The second category will consider the ratios of the neutron capture rates in ^{238}U to the total fission rates ($C8/F$). The proposed method is based on a fuel rod gamma scanning technique. The apparatus available at the IPEN/MB-01 facility has an opening collimator of 1.0 cm. These experiments were mainly proposed to fulfill a specific need to verify the new ^{238}U nuclear data with spectral indices that does not require any sort of calculated correction factors. The final whole set of experimental data was recently evaluated and approved as benchmark data for inclusion in the IRPhE Handbook (Dos Santos et al., 2012).

The IPEN/MB-01 reactor is a zero power-critical facility especially designed for measurement of a wide variety of reactor physics parameters to be used as a benchmark experimental data for checking the calculation methodologies and related nuclear data libraries commonly used in the field of reactor physics. This facility consists of an array of 28×26 UO_2 fuel rods, 4.3% enriched and clad by stainless steel (type 304) inside of a light water tank. A complete description of the IPEN/MB-01 reactor may be found elsewhere (Dos Santos et al., 2004).

2. Geometry of the experiment configuration and measurement procedure

The experiments employed the standard 28×26-fuel-rod configuration as shown in Fig. 1. Experimental fuel rods with the same description as the IPEN/MB-01 core fuel rods were used throughout the measurements. The reactivity was controlled by two control banks (BC1 and BC2 in Fig. 1) of Ag–In–Cd alloy. The safety banks of B_4C are kept at its completely removal position of 135% (the absorber is at 35% of the active core length above the active core) during the whole set of measurements. Therefore, when the safety banks are in the totally withdrawn position, they have very little impact on the reactivity of the system. All geometric and material data are described in Section 1.2 of LEU-COMP-THERM-077 (Dos Santos et al., 2004); however these spectral indices measurements had no baffle plates surrounding the core.

The experiment was set up in the following way: An experimental fuel rod was placed at the central position of the core; more precisely in the position M14 of Fig. 1. Initially, two positions along its active axial direction are chosen such that the reaction rates (^{238}U captures and total fissions) show nearly symmetric values. After that, one position was kept bare while the other one was covered with a sleeve of Cadmium of specific size and thickness. The requirement for the selection of the two axial positions is that when the Cadmium sleeve is introduced the reaction rate in the other symmetric position remains nearly unchanged from its original value. This was the basic principle for the selection of the symmetric points. This experimental fuel rod is subsequently irradiated at the central region of the IPEN/MB-01 core for a period of 1 h in a power of 100 W. The quantities measured are the detector countings of ^{239}Np and ^{143}Ce at the end of irradiation by a gamma scanning equipment. This scanning equipment is the same as used for the determination of the fission rates of Sections 1.7 and 1.8 of IPEN(MB01)-LWR-RESR-001 (Dos Santos et al., 2012). The spectral indices are derived from these detector countings. Since the ^{239}Np and ^{143}Ce gamma countings of the bare and the Cadmium covered regions are obtained in the same reactor operation, the experiment is also not sensitive to the power normalization and even to the power ramps.

3. Method to measure the spectral indices

The essence of the proposed method to measure the spectral indices starts with the works of Nakajima (Nakajima et al., 1994a,b). According to Nakajima the ^{238}U capture rate ($C8$) and total fission rate (F) inferred from the scanning detector countings are given respectively by Eqs. (1) and (2) as:

$$C8 = \frac{\lambda_{U9} - \lambda_{Np}}{\lambda_{U9}} \cdot \frac{\lambda_{Np} \cdot N_{Np}}{f_{\gamma Np} \cdot g_{Np} \cdot \eta_{Np} \cdot [1 - \exp(-\lambda_{Np} t_I)] \cdot \exp(-\lambda_{Np} t_E) \cdot [1 - \exp(-\lambda_{Np} t_C)]}, \tag{1}$$

$$F = \frac{\lambda_{Ce} \cdot N_{Ce}}{\bar{Y}_{Ce} \cdot f_{\gamma Ce} \cdot g_{Ce} \cdot \eta_{Ce} \cdot [1 - \exp(-\lambda_{Ce} t_I)] \cdot \exp(-\lambda_{Ce} t_W) \cdot [1 - \exp(-\lambda_{Ce} t_C)]}, \tag{2}$$

where λ_i is the decay constant of nuclide i (Np for ^{239}Np, U9 for ^{239}U, and Ce for ^{143}Ce), N_i is the photopeak intensity (countings) for a characteristic transition of nuclide i at the end of the irradiation, g_i is the gamma emission probability of nuclide i, $f_{\gamma i}$ is the fuel rod gamma self-shielding factor of nuclide i, η_i is the gamma detector efficiency for nuclide i, t_I, t_W, t_C are respectively the irradiation time, the waiting time, and the counting time, and $\bar{Y}_{Ce}$ is the effective ^{143}Ce fission yield defined by:

$$\bar{Y}_{Ce} = \frac{Y_{Ce}^{25}(\sum_f \Phi)_{25} + Y_{Ce}^{28}(\sum_f \Phi)_{28}}{(\sum_f \Phi)_{25} + (\sum_f \Phi)_{28}}, \tag{3}$$

where Y_{Ce}^{i} is the ^{143}Ce fission yield for nuclide i (25 for ^{235}U and 28 for ^{238}U) and $(\sum_f \Phi)_i$ is the fission rate of nuclide i.

The spectral indices $^{28}\rho^*$ and $^{25}\delta^*$ are defined as:

$$SI = \frac{\text{Perturbed Value}}{\text{Unperturbed Value} - \text{Perturbed Value}}, \tag{4}$$

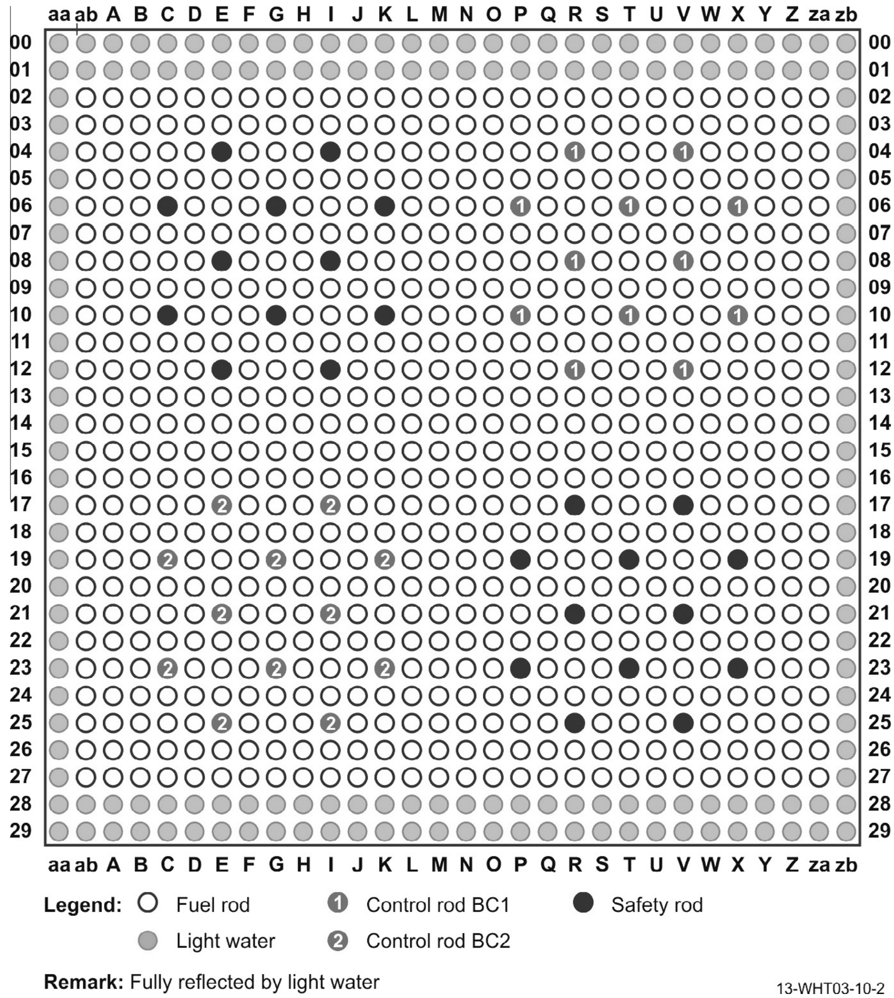

Fig. 1. IPEN/MB-01 reactor core configuration for the spectral index measurements.

where SI represents the spectral index (either $^{28}\rho^*$ or $^{25}\delta^*$), *Perturbed Value* is either the ^{238}U capture rate or the ^{235}U fission rate in the irradiated fuel rod at the Cadmium covered position, and the *Unperturbed Value* is the same respective quantity in the irradiated fuel rod at the bare position.

Substituting Eqs. (1) and (2) into Eq. (4), and noting that several terms are cancelled, the spectral index SI becomes:

$$SI = \frac{1}{\frac{f^*_{\gamma i} \cdot \eta^*_i}{\varepsilon_i \cdot f_{\gamma i} \cdot \eta_i} \cdot R_{\text{Cd}} - 1}, \tag{5}$$

where all the physical quantities with superscript (*) refer to the Cadmium covered region and unless otherwise stated the quantities without superscript refers to the bare case, R_{Cd} is the Cadmium ratio defined as the ratio between the detector countings at the end of the irradiation in the bare position to that in the Cadmium covered position, ε_i = 1.0 for $^{28}\rho^*$ and $\varepsilon_i = \frac{F^*_{25} \bar{Y}_{\text{Ce}}}{F_{25} \bar{Y}^*_{\text{Ce}}}$ for $^{25}\delta^*$, and F_{25} is the ^{235}U fission rate fraction.

Eq. (5) is the basic equation for the measurement of the spectral indices$^{28}\rho^*$ and $^{25}\delta^*$. The measured quantities are the Cadmium ratio (R_{Cd}) and $\frac{f_{\gamma i} \cdot \eta_i}{f^*_{\gamma i} \cdot \eta^*_i}$, the ratios of the detector efficiencies and the fuel rod self-shielding factors. ε_i is a calculated quantity used only in the $^{25}\delta^*$ case.

The spectral index as defined by Eq. (5) is the ratio of the epithermal to thermal reaction rates. This applies either to the ^{238}U neutron capture or to the ^{235}U fission. In the case of ^{238}U neutron capture this spectral index is the $^{28}\rho^*$ and in the case of ^{235}U fission it is the $^{25}\delta^*$. These are very classical spectral indices measured in several facilities (Bitelli and Dos Santos, 2002; Hardy, 1983) with the utilization of depleted uranium foils for $^{28}\rho^*$ and highly enriched uranium foils for $^{25}\delta^*$. The uranium foils are normally wrapped with thin aluminum foils in order to prevent fission products from the neighboring pellets to enter into the foils and contribute to the countings. The conversion of the measured foil reaction into the pellet reaction (either ^{238}U capture or ^{235}U fissions) requires the introduction of calculated correction factors (Sher and Fiarman, 1976). Some other corrections must be applied for the power ramp and the power normalization due to the fact that the bare and the Cadmium covered cases are run in distinct reactor operations. More correction factors are needed to correct the thermal cutoff to 0.625 eV (Sher and Fiarman, 1976).

The purpose of the experiments performed at IPEN/MB-01 reactor facility was to avoid the introduction of such calculated correction factors, mainly for the case of ^{238}U captures. This aspect gave to the IPEN/MB-01 experiments an excellent quality and free of possible bias due to the calculated correction factors. The superscript (*) indicates that these spectral indices refer to the perturbed case; i.e., the spectral indices $^{28}\rho^*$ and $^{25}\delta^*$ will depend on the location of the symmetric points and the geometric characteristics of the Cadmium sleeve. There will not be any transformation to the unperturbed case and even the transformation to the thermal cutoff of 0.625 eV. The experiments are calculated exactly as they were performed.

The spectral index $C8/F$ is defined dividing Eqs. (1) and (2). The final result is:

$$\frac{C8}{F} = K\frac{f_{\gamma \mathrm{Ce}} \cdot \eta_{\mathrm{Ce}} \bar{Y}_{\mathrm{Ce}}}{f_{\gamma \mathrm{Np}} \cdot \eta_{\mathrm{Np}}} \frac{N_{\mathrm{Np}}}{N_{\mathrm{Ce}}}, \tag{6}$$

where

$$K = \left(\frac{\lambda_{\mathrm{U9}} - \lambda_{\mathrm{Np}}}{\lambda_{\mathrm{U9}}}\right) \frac{\lambda_{\mathrm{Np}} g_{\mathrm{Ce}}[1 - \exp(-\lambda_{\mathrm{Ce}} t_w)] \exp(-\lambda_{\mathrm{Ce}} t_I)[1 - \exp(-\lambda_{\mathrm{Ce}} t_m)]}{\lambda_{\mathrm{Ce}} g_{\mathrm{Np}}[1 - \exp(-\lambda_{\mathrm{Np}} t_w)] \exp(-\lambda_{\mathrm{Np}} t_I)[1 - \exp(-\lambda_{\mathrm{Np}} t_m)]},$$

and "exp" represents the exponential function.

Eq. (6) is applied to the bare and Cadmium covered positions and the spectral index $C8/F$ is determined accordingly. The measured quantities in this equation is $\frac{N_{\mathrm{Np}}}{N_{\mathrm{Ce}}}$, and the ratio $\frac{f_{\gamma \mathrm{Ce}}}{f_{\gamma \mathrm{Np}}} \cdot \frac{\eta_{\mathrm{Ce}}}{\eta_{\mathrm{Np}}} \cdot \bar{Y}_{\mathrm{Ce}}$, given by Eq. (3), and K are calculated quantities. $\bar{Y}_{\mathrm{Ce}}$ depends on the characteristics of the measured positions (bare and Cadmium covered) and K depends on the operational and measurement conditions and on several physical data of the gamma emission nuclide (either ^{143}Ce or ^{239}Np).

An important factor of Eq. (5) is $\frac{f_{\gamma i} \cdot \eta_i}{f^*_{\gamma i} \cdot \eta^*_i}$. The experimental determination of this quantity was addressed in the following way.

The efficiency of the HPGe detector is a complex function of the geometry of the radioactive source, its distance to the detector as well as the gamma energy spectrum (or energy) emitted by this source. The detector efficiency can be written as a product of two terms. One term that is only gamma energy dependent and a second term that is dependent on the spatial source distribution, its distance to the detector and the gamma self-shielding factor inside of the source. For the spectral indices $^{28}\rho^*$ and $^{25}\delta^*$, the energy dependence of the ratio of the detector efficiencies can be ignored because the ratio of the detector efficiency is considered only for the same radioactive isotope; either ^{239}Np or ^{143}Ce. Consequently, only the spatial details and the gamma self-shielding factor of the radioactive source will be of interest for these spectral indices. For the specific case under consideration, the radial reaction rate profiles inside of the UO_2 pellets in the two regions being measured (bare and Cadmium covered) are responsible for different values of detector efficiency. The gamma self-shielding factors for these two situations will also require a special treatment mainly for the $^{28}\rho^*$ case. From the experimental point of view, detector efficiency and gamma self-shielding factor cannot be decoupled; both effects occur at the same time. Therefore, the proposed method here is to determine $\frac{f_{\gamma \mathrm{Ce}} \cdot \eta_{\mathrm{Ce}}}{f^*_{\gamma \mathrm{Np}} \cdot \eta^*_{\mathrm{Np}}}$ without decoupling these effects.

$\frac{f_{\gamma i} \cdot \eta_i}{f^*_{\gamma i} \cdot \eta^*_i}$ of the gamma scanning equipment was determined considering the irradiations of UO_2 thin disks (same diameter as the fuel pellet and small thickness) in the interior of a dismountable fuel rod. These UO_2 disks were obtained from the pellets used in the fuel rods. A pellet was cut by a special tool into very thin disks. These disks were placed between fuel pellets aiming to measure the reaction rates inside of the fuel rod. Since these thin disks have the same composition and diameter of the original UO_2 pellet, there will not be any need to apply any correction for the disk perturbation. In fact there will not be any perturbation due to the insertion of these disks between pellets. The axial positions of the UO_2 disks were as close as possible to those of the experimental fuel rod used in the scanning equipment. $\frac{f_{\gamma i} \cdot \eta_i}{f^*_{\gamma i} \cdot \eta^*_i}$ of the gamma scanning equipment can be found by noting that this quantity is equal to the ratio of the Cadmium ratio of the UO_2 disks to the Cadmium ratio of the dismountable fuel rod in the same axial disk positions but now measured by the gamma scanning equipment. In the previous case, the axial disk position is the center of the 1 cm length seen by the HPGe detector of the gamma scanning equipment. This reasoning was applied for the two different Cadmium sleeves used in this work.

For the spectral index $C8/F$, the ratio of detector efficiencies is somehow more complicated because both the gamma energy dependence and the details of space distribution of the source as well as its distance to the detector are important. Particularly in this case the radial distribution of the gamma source is due to the different nuclear reaction; neutron capture in ^{238}U and neutron fission in ^{235}U. For this reason special care was taken to take this effect into consideration as follow.

The systems for gamma spectrometry (UO_2 disk or fuel rod scanning) were gamma energy calibrated employing ^{152}Eu and ^{133}Ba standard sources. The measured data were least-square fitted in a first order polynomial function as:

$$\ln(\eta) = A + B \cdot \ln(E), \tag{7}$$

where η is the detector efficiency, E is the gamma energy, and A and B are constants arising from the least-square fit of the calibration data. The detector efficiency at the gamma energies emitted by ^{239}Np (277.6 keV) and by ^{143}Ce (293.4 keV) could then be determined in a straightforward fashion from Eq. (7) once A and B are known from the least-square approach.

The uncertainty analysis associated with the determination of the detector efficiency was addressed employing a standard least-square approach (Smith, 1991; ORIGIN-6.1). The uncertainty associated to the detector efficiency is given by: $\sigma^2_\eta = \Gamma^+ V_\sigma \Gamma$ (Smith, 1991; ORIGIN-6.1). The vector Γ and the matrix V_σ are defined and extensively discussed in Refs. Bevington (1969) and Smith (1991).

Consider the function RE; the ratio of the detector efficiencies $\frac{\eta^E_{\mathrm{Ce}}}{\eta^E_{\mathrm{Np}}}$ defined by:

$$RE = \eta_1/\eta_2, \tag{8}$$

where η_1 is the detector efficiency at 277.6 keV and η_2 is the same quantity at 293.4 keV.

The variance of RE can be found employing a standard error propagation as:

$$\sigma^2_{RE} = \left(\frac{\partial RE}{\partial \eta_1}\right)^2 \sigma^2_{\eta 1} + \left(\frac{\partial RE}{\partial \eta_2}\right)^2 \sigma^2_{\eta 2} + 2\left(\frac{\partial RE}{\partial \eta_1}\right)\left(\frac{\partial RE}{\partial \eta_2}\right)\sigma^2_{\eta_1 \eta_2}, \tag{9}$$

$\sigma^2_{\eta_1 \eta_2}$ represents the correlation between η_1 and η_2 is given by:

$$\sigma^2_{\eta_1 \eta_2} = \Gamma^+(\eta_1) V_\sigma \Gamma(\eta_2), \tag{10}$$

where $\Gamma^+(\eta_1)$ is the transpose of Γ vector at energy 277.6 keV and $\Gamma(\eta_2)$ is the Γ vector at energy 293.4 keV.

The ratio $\frac{f_{\gamma i} \cdot \eta_i}{f^*_{\gamma i} \cdot \eta^*_i}$ due to the spatial source distribution and due to the fuel rod self-shielding factor for the spectral index $C8/F$ was found in the following way. Consider Eq. (6) rewritten here as:

$$\frac{C8}{F} = K \frac{\eta^E_{\mathrm{Ce}}}{\eta^E_{\mathrm{Np}}} \frac{\bar{Y}_{\mathrm{Ce}}}{CF} \frac{N_{\mathrm{Np}}}{N_{\mathrm{Ce}}}, \tag{11}$$

where $\frac{\eta^E_{\mathrm{Ce}}}{\eta^E_{\mathrm{Np}}}$ is the ratio of the energy dependent detector efficiency given by Eq. (8) for the scanning equipment, CF is an experimental correction factor for the detector efficiencies defined as:

$$CF = \frac{(C8/F)_{\mathrm{Disk}}}{(C8/F)_{\mathrm{Fuel\ rod}}}, \tag{12}$$

or more explicitly

$$CF = \frac{\left(\frac{\eta^E_{\mathrm{Np}}}{\eta^E_{\mathrm{Ce}}}\right)_{\mathrm{Disk}}}{\left(\frac{\eta^E_{\mathrm{Np}}}{\eta^E_{\mathrm{Ce}}}\right)_{\mathrm{Fuel\ rod}}} \cdot \left(\frac{\left(\frac{N_{\mathrm{Np}}}{N_{\mathrm{Ce}}}\right)_{\mathrm{Disk}}}{\left(\frac{N_{\mathrm{Np}}}{N_{\mathrm{Ce}}}\right)_{\mathrm{Fuel\ rod}}}\right), \tag{13}$$

The factor *CF* is an experimental correction factor that takes into account the spatial dependence of the radial reaction rate profiles and a relationship between the efficiency of the gamma UO_2 disk spectrometry system and the same quantity for the fuel rod system, and the gamma self-shielding factor. It should be stressed again here that for the UO_2 disk spectrometry there is no need to take into account any dependence of the detector efficiency ratio on the radial distribution of the gamma source. The gamma self-shielding correction in the fuel disk was found to be negligible. Contrary to that, the detector efficiency of the fuel rod scanning system has to account for the radial profiles of two distinct nuclear reactions; namely neutron capture in ^{238}U and neutron fissions in ^{235}U as well as the gamma self-shielding occurring inside of the fuel pellet. This part of the detector efficiency ratio is taken into account by Eq. (13).

The selection of the symmetric points of the fuel rod to be used in the experimental approach was chosen after a very tedious analysis. The conclusion reached for the best positions was the axial points located at 10.0 cm and 35.0 cm from the bottom of the fuel rod active length. These axial points represent the center of a cylinder of 1.0 cm length and whose center is the center of the pellet. The Cadmium sleeve is centered at the axial position located at 35.0 cm.

4. Experimental results

The first part of the experimental process was to calibrate both the detector systems (disk and fuel rod) employing ^{152}Eu and ^{133}Ba standard sources. This calibration was accomplished in a straightforward fashion and the uncertainty analysis was performed employing the procedure described in the previous section. The quantities of interest for this work are presented in Table 2.

The basic experimental quantity measured in this work is the gamma energy spectra emitted by the fission products, actinides and structural nuclides contained in the UO_2 disk or in the experimental fuel rod. The gamma energy spectra were measured as a function of decay time starting 24 h after the reactor shutdown by two distinct HPGe detectors; one for the UO_2 disk and another one for the gamma scanning equipment. From these spectra quantities like countings of a specific photopeak of a specific nuclide like ^{239}Np can be inferred by the software MAESTRO software.[1] The ^{143}Ce and ^{239}Np characteristic gamma countings were corrected for the detector dead-time. The whole process for each selected axial position consists of 72 measurements, each of which with a 3600 s counting time. The intensities (areas/countings) of ^{143}Ce and the ^{239}Np photopeaks were least-square fitted as an exponential function as a function of the decay time employing the ORIGIN 6.0 (ORIGIN-6.1) software. The only fitted datum is the amplitude coefficient which is the intensity (counting/amplitude) of the specific radioactive nuclide at the end of the irradiation. The decay constants used in the exponential function were 0.01226 (h^{-1}) (Reus and Westmeier, 1983) for ^{239}Np and 0.02097 (h^{-1}) (Reus and Westmeier, 1983) 16] for ^{143}Ce. Whenever the word countings is mentioned in this work it will refer to the detector countings at the end of irradiation.

The countings are, respectively, for the bare and in Cadmium covered positions for the experimental and dismountable fuel rods. Other quantities like the spectral indices of this evaluation are considered derived quantities. The evaluation carried out here went through several steps up to the derived quantities and the establishment of the corresponding uncertainties. The experimental approach was very lengthy and laborious. Only the final results are shown here.

[1] ORTEC MAESTRO-32, Version 6.0, Ametek Advanced Measurement Technology, Inc., 2004.

Table 2
Detector efficiency at the gamma energies emitted by ^{239}Np (277.6 keV) and by ^{143}Ce (293.4 keV).

Detector system	η_{Np} (277.6 keV) 1σ (%)	η_{Ce} (293.4 keV) 1σ (%)	$\frac{\eta_{Np}\ (277.6\ keV)}{\eta_{Ce}\ (293.4\ keV)}$ 1σ (%)
UO_2 disk	1.2652×10^{-2} (1.51)	1.2095×10^{-2} (1.44)	1.046 (0.076)
Fuel rod scanning	7.69069×10^{-4} (1.84)	7.06689×10^{-4} (1.80)	1.088 (0.625)

The uncertainty propagation was addressed in the standard way as:

$$\sigma_\omega^2 = \left(\frac{\partial\omega}{\partial x}\right)^2 \sigma_x^2 + \left(\frac{\partial\omega}{\partial y}\right)^2 \sigma_y^2, \tag{14}$$

where ω represents a function relating the countings considered in the determination of a specific spectral index, *x* and *y* represents the pair of countings, and σ_x^2, and σ_y^2 represents the square of the standard deviation of the mean of the *x* and *y* countings, respectively. No correlation was assumed between the variables *x* and *y*.

One dismountable fuel rod was used throughout of the experiments and for each irradiation two UO_2 disks were inserted in its interior in the axial positions as close as possible to the symmetric points (10.0 and 35.0 cm). The disks were cut in pairs. This pair of UO_2 disks was cut in such a way as to allow very small mass and thickness variations between them. The UO_2 disk pair thicknesses vary from nearly 0.5 mm to 1.7 mm. Table 3 shows details of the UO_2 disks. The thickness of the disks was not a measured quantity; it was derived from the mass of the disk and the density of UO_2 (10.1771 ± 0.1018 g/cm^3). The uncertainty in the UO_2 is one standard deviation (1σ).

Table 3
Characteristics of the UO_2 disks.

Pair	Disk	Mass (g)	Thickness (mm)
1	1	0.3443 ± 0.0002	0.5962 ± 0.0003
	2	0.3446 ± 0.0002	0.5962 ± 0.0003
2	3	0.3994 ± 0.0002	0.6915 ± 0.0003
	4	0.3995 ± 0.0002	0.6918 ± 0.0003
3	5	0.4111 ± 0.0002	0.7118 ± 0.0003
	6	0.4112 ± 0.0002	0.7121 ± 0.0003
4	7	0.4208 ± 0.0002	0.7286 ± 0.0003
	8	0.4208 ± 0.0002	0.7287 ± 0.0003
5	9	0.4936 ± 0.0002	0.8547 ± 0.0003
	10	0.4937 ± 0.0002	0.8549 ± 0.0003
6	11	0.5266 ± 0.0002	0.9118 ± 0.0003
	12	0.5267 ± 0.0002	0.9120 ± 0.0003
7	13	0.5560 ± 0.0002	0.9627 ± 0.0003
	14	0.5560 ± 0.0002	0.9627 ± 0.0003
8	15	0.5645 ± 0.0002	0.9776 ± 0.0003
	16	0.5648 ± 0.0002	0.9780 ± 0.0003
9	17	0.6323 ± 0.0002	1.0949 ± 0.0003
	18	0.6325 ± 0.0002	1.0952 ± 0.0003
10	19	0.6965 ± 0.0002	1.2061 ± 0.0003
	20	0.6966 ± 0.0002	1.2063 ± 0.0003
11	21	0.7848 ± 0.0002	1.3590 ± 0.0003
	22	0.7849 ± 0.0002	1.3591 ± 0.0003
12	23	0.8443 ± 0.0002	1.4620 ± 0.0003
	24	0.8444 ± 0.0002	1.4621 ± 0.0003
13	25	0.8542 ± 0.0002	1.4792 ± 0.0003
	26	0.8543 ± 0.0002	1.4793 ± 0.0003
14	27	0.9283 ± 0.0002	1.6074 ± 0.0003
	28	0.9285 ± 0.0002	1.6077 ± 0.0003
15	29	0.9902 ± 0.0002	1.7147 ± 0.0003
	30	0.9905 ± 0.0002	1.7152 ± 0.0003
16	31	0.3395 ± 0.0002	0.5879 ± 0.0003
	32	0.3395 ± 0.0002	0.5879 ± 0.0003

The UO_2 disks were inserted between the 10th and 11th fuel pellets and between the 34th and 35th fuel pellets, which for the dismountable fuel rod used in the experiment correspond, respectively, to the axial positions 10.4 cm and 35.6 cm from the bottom of the active length of this fuel rod. These axial positions were the closest ones to the symmetric points chosen previously.

The system of gamma spectrometry of the UO_2 disks was calibrated in energy by a standard Eu source. Since the foils are very thin and placed perpendicular to the detector, there is no need to make any correction to the detector efficiency due to the different radial reaction rate profiles for the disks placed in the bare and Cadmium covered positions. Also, there is no need to take into the gamma attenuation in the disk because these gamma attenuation factors are in the numerator and denominator of $\frac{f_{\gamma i}}{f^*_{\gamma i}}$ and they cancel because they are almost identical. Therefore for the UO_2 disks the radial reaction rate profile contribution to the ratio $\frac{f_{\gamma i}\cdot\eta_i}{f^*_{\gamma i}\cdot\eta^*_i}$ is equal to one.

The procedure to obtain the ratio $\frac{f_{\gamma i}\cdot\eta_i}{f^*_{\gamma i}\cdot\eta^*_i}$ for the gamma scanning equipment was to perform two types of irradiations with the dismountable fuel rod. The first irradiation involved the UO_2 disks inserted at positions 10.4 and 35.6 cm from the bottom of the active length. The second irradiation involved the dismountable fuel rod without the UO_2 disks but now this rod was taken to the scanning equipment. The gamma spectra emitted by the dismountable fuel rod was measured in the region of 1.0 cm length centered in the axial positions 10.4 and 35.6 cm of this fuel rod. The ratio $\frac{f_{\gamma i}\cdot\eta_i}{f^*_{\gamma i}\cdot\eta^*_i}$ needed for ${}^{28}\rho^*$ and ${}^{25}\delta^*$ determination is the ratio of the Cadmium ratio of these two sets of measurements.

Table 4 shows the results for the Cadmium ratio and ${}^{28}\rho^*$ for a Cadmium sleeve 0.55 mm thickness and 5.0 cm length employing the several pairs of UO_2 disks of this work. These data are also shown in a graphical form in Fig. 2. In Table 4 and in the following tables T represents the UO_2 disk thickness. The ${}^{239}Np$ countings at the end of the irradiation were estimated from the least-square fit of an exponential function of several measurements of the UO_2 disks. Consequently the counting uncertainties are smaller than their corresponding square root. This reasoning is applied to all tables in this section. Still in Table 4, ${}^{28}R_{Cd}$ represents the Cadmium ratio for the ${}^{239}Np$ countings. The critical control bank withdrawn position for these cases is 32.487 cm.

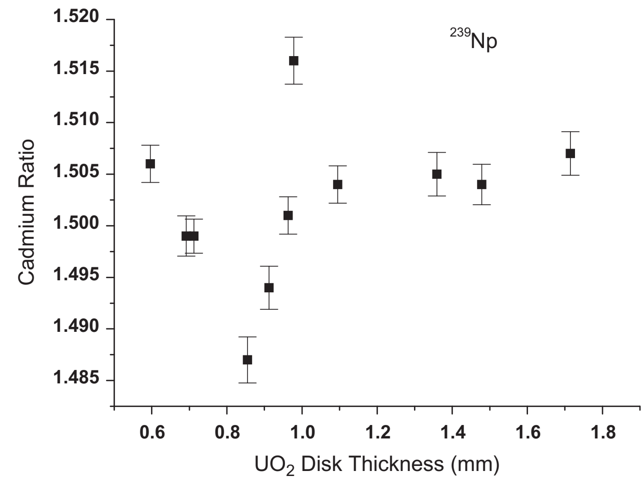

Fig. 2. ${}^{238}U$ Cadmium ratio variation as a function of the UO_2 disk thickness.

Fig. 2 shows that the ${}^{238}U$ Cadmium ratio as a function of the UO_2 disk thickness does not follow any specific law. The data shows a random behavior. Due to that, an average value for the 11 irradiations was assumed as the final value. Table 4 shows the average value and the corresponding uncertainty. The same procedure was adopted for the Cadmium sleeve of thicknesses 1.10 mm. The final results for this case are shown in Table 5.

The determination of the Cadmium ratio for ${}^{143}Ce$ countings follows basically the same approach and the raw data arises from the same gamma spectra measured for ${}^{239}Np$. Tables 6 and 7 show the final results for the Cadmium sleeve thickness of 0.55 and 1.10 mm, respectively. Here R_{Cd} is the Cadmium ratio for the ${}^{143}Ce$ countings.

The Cadmium ratios of the dismountable fuel rod in the exact positions of the irradiation of the UO_2 disks (bare position 10.4 cm and Cadmium covered position 35.6 cm) were measured employing the scanning equipment. The results are shown in Tables 8 and 9 for the ${}^{239}Np$ cases and in Tables 10 and 11 for the ${}^{143}Ce$ cases. Four distinct irradiations were performed for each Cadmium sleeve thickness.

Table 12 shows the final values of the ratio $\frac{f_{\gamma i}\cdot\eta_i}{f^*_{\gamma i}\cdot\eta^*_i}$ for ${}^{239}Np$ and ${}^{143}Ce$. ${}^{28}F_{cor}$ represents the ratio $\frac{f_{\gamma i}\cdot\eta_i}{f^*_{\gamma i}\cdot\eta^*_i}$ for ${}^{239}Np$ and ${}^{25}F_{cor}$ represents the same ratio for ${}^{143}Ce$.

Table 4
Countings of the ${}^{239}Np$ in the UO_2 disks and inferred spectral index for a Cadmium sleeve of 0.55 mm thickness and 5.0 cm length.

T (mm)	Fuel rod axial position		${}^{28}R_{Cd}$
	Bare	Cd sleeve	σ (%)
1.715	5.2475×10^5 (664)	3.4815×10^5 (224)[b]	1.507 (0.1)
1.479	4.7470×10^5 (551)	3.1563×10^5 (188)	1.504 (0.1)
1.359	4.5115×10^5 (534)	2.9975×10^5 (199)	1.505 (0.1)
1.095	3.8660×10^5 (401)	2.5697×10^5 (158)	1.504 (0.1)
0.978	3.5152×10^5 (362)	2.3184×10^5 (263)	1.516 (0.2)
0.963	3.5049×10^5 (394)	2.3347×10^5 (124)	1.501 (0.1)
0.912	3.2882×10^5 (332)	2.2011×10^5 (218)	1.494 (0.1)
0.855	3.1786×10^5 (457)	2.1371×10^5 (123)	1.487 (0.2)
0.712	2.7315×10^5 (227)	1.8227×10^5 (121)	1.499 (0.1)
0.692	2.6620×10^5 (216)	1.7753×10^5 (176)	1.499 (0.1)
0.596	2.3845×10^5 (244)	1.5832×10^5 (103)	1.506 (0.1)
Average			1.502 (0.04)

Table 5
Countings of the ${}^{239}Np$ in the UO_2 disks and inferred spectral index for a Cadmium sleeve of 1.10 mm thickness and 5.0 cm length.

T (mm)	Fuel rod axial position		${}^{28}R_{Cd}$
	Bare	Cd sleeve	σ (%)
0.692	2.6362×10^5 (209)	$1.7118E5 \times 10^5$ (185)	1.540 (0.1)
0.729	2.7149×10^5 (162)	1.7735×10^5 (162)	1.531 (0.1)
0.855	3.1401×10^5 (278)	2.0337×10^5 (273)	1.544 (0.2)
0.912	3.3434×10^5 (269)	2.1334×10^5 (272)	1.567 (0.2)
Average			1.546 (0.1)

Table 6
Countings of the ^{143}Ce in the UO_2 disks and inferred spectral index for a Cadmium sleeve of 0.55 mm thickness and 5.0 cm length.

T (mm)	Fuel rod axial position		R_{Cd}
	Bare	Sleeve	σ (%)
1.715	4.8519×10^5 (2884)	6.7324×10^4 (239)	7.207 (0.7)
1.479	4.4284×10^5 (1702)	6.0210×10^4 (274)	7.355 (0.6)
1.359	4.1757×10^5 (1714)	5.6828×10^4 (236)	7.348 (0.6)
1.095	3.5428×10^5 (1466)	4.8781×10^4 (209)	7.263 (0.6)
0.978	3.1729×10^5 (551)	4.3215×10^4 (105)	7.342 (0.3)
0.963	3.1853×10^5 (1288)	4.4139×10^4 (172)	7.216 (0.6)
0.912	2.9927×10^5 (609)	4.0998×10^4 (94)	7.300 (0.3)
0.855	2.8893×10^5 (1280)	3.9732×10^4 (158)	7.272 (0.6)
0.712	2.4629×10^5 (517)	3.3809×10^4 (85)	7.285 (0.3)
0.692	2.3853×10^5 (410)	3.2689×10^4 (100)	7.297 (0.4)
0.596	2.1315×10^5 (678)	2.9273×10^4 (80)	7.281 (0.4)
Average			7.288 (0.2)

Table 7
Countings of the ^{143}Ce in the UO_2 disks and inferred spectral index for a Cadmium sleeve of 1.10 mm thickness and 5.0 cm length.

T (mm)	Fuel rod axial position		R_{Cd}
	Bare	Sleeve	σ (%)
0.692	2.3498×10^5 (386)	3.0084×10^4 (96)	7.811 (0.4)
0.729	2.4335×10^5 (412)	3.1033×10^4 (99)	7.841 (0.4)
0.855	2.8302×10^5 (465)	3.6135×10^4 (96)	7.832 (0.3)
0.912	3.0188×10^5 (458)	3.7964×10^4 (132)	7.952 (0.4)
Average			7.859 (0.2)

Table 8
Countings of the ^{239}Np in the UO_2 fuel rod and inferred spectral index for a Cadmium sleeve of 0.55 mm thickness and 5.0 cm length in the positions 10.4 cm and 35.6 cm.

Irrad.	Fuel rod axial position		$^{28}R_{Cd}$
	Bare	Sleeve	σ (%)
1	8.0358×10^4 (139)	5.3554×10^4 (56)	1.500 (0.2)
2	8.1317×10^4 (111)	5.4612×10^4 (56)	1.489 (0.2)
3	8.1341×10^4 (141)	5.5003×10^4 (59)	1.479 (0.2)
4	8.1315×10^4 (140)	5.5250×10^4 (50)	1.472 (0.2)
Average			1.485 (0.1)

Table 9
Countings of the ^{239}Np in the UO_2 fuel rod and inferred spectral index for a Cadmium sleeve of 1.10 mm thickness and 5.0 cm length in the positions 10.4 cm and 35.6 cm.

Irrad.	Fuel rod axial position		$^{28}R_{Cd}$
	Bare	Sleeve	σ (%)
1	7.0001×10^4 (109)	4.5230×10^4 (47)	1.548 (0.2)
2	7.3411×10^4 (126)	4.8387×10^4 (54)	1.517 (0.2)
3	7.9131×10^4 (142)	5.1441×10^4 (55)	1.538 (0.2)
4	7.0641×10^4 (116)	4.5498×10^4 (52)	1.553 (0.2)
Average			1.539 (0.1)

Table 10
Countings of the ^{143}Ce in the UO_2 fuel rod and inferred spectral index for a Cadmium sleeve of 0.55 mm thickness and 5.0 cm length in the positions 10.4 cm and 35.6 cm.

Irrad.	Fuel rod axial position		R_{Cd}
	Bare	Sleeve	σ (%)
1	6.2956×10^4 (268)	8.5218×10^3 (46)	7.388 (0.6)
2	6.2790×10^4 (292)	8.4613×10^3 (49)	7.421 (0.7)
3	6.2960×10^4 (285)	8.5422×10^3 (50)	7.370 (0.7)
4	6.3426×10^4 (295)	8.5666×10^3 (49)	7.404 (0.7)
Average			7.396 (0.35)

Table 11
Countings of the ^{143}Ce in the UO_2 fuel rod and inferred spectral index for a Cadmium sleeve of 1.10 mm thickness and 5.0 cm length in the positions 10.4 cm and 35.6 cm.

Irrad.	Fuel rod axial position		R_{Cd}
	Bare	Sleeve	σ (%)
1	6.0881×10^4 (256)	7.5562×10^3 (40)	8.057 (0.7)
2	6.1177×10^4 (279)	7.5526×10^3 (44)	8.100 (0.7)
3	6.2380×10^4 (252)	7.8120×10^3 (49)	7.985 (0.8)
4	6.1218×10^4 (279)	7.6991×10^3 (41)	7.951 (0.7)
Average			8.023 (0.4)

Table 12
Ratio $\frac{f_{\gamma i} \cdot \eta_i}{f^*_{\gamma i} \cdot \eta^*_i}$ for the two types of Cadmium sleeve.

T (mm)	^{239}Np			^{143}Ce		
	$^{28}R_{Cd}$ rod σ (%)	$^{28}R_{Cd}$ disk σ (%)	$^{28}F_{cor}$ σ (%)	$^{25}R_{Cd}$ rod σ (%)	$^{25}R_{Cd}$ disk σ (%)	$^{25}F_{cor}$ σ (%)
0.55	1.485 (0.1)	1.502 (0.04)	0.989 (0.1)	7.396 (0.4)	7.288 (0.2)	1.015 (0.4)
1.10	1.539 (0.1)	1.546 (0.1)	0.996 (0.1)	8.023 (0.4)	7.859 (0.2)	1.021 (0.4)

The same raw experimental data (i.e., countings of ^{239}Np and ^{143}Ce) from the experiments mentioned previously and presented in Tables 9–11 are used for the determination of the ratios N_{Np}/N_{Ce} and consequently to the correction factor *CF* employing Eq. (13). These ratios together with the ratio of detector efficiencies for ^{239}Np and ^{143}Ce are then used for the determination of *CF*. Tables 13 and 14 show the correction factor *CF* employing Eq. (13) for the bare and Cadmium covered positions respectively.

Table 13
Ratio of detector efficiencies for the $C8/F$ experiment for the Cadmium sleeve of 5.0 cm length in the bare position.

Cadmium sleeve thickness (mm)	Bare position ^{239}Np/^{143}Ce Disk/fuel rod σ (%)	Ratio of η_{Np} (277.6 keV)/η_{Ce} (293.4 keV) Disk/fuel rod (1σ (%))	CF_{Bare} σ (%)
0.55	1.172	0.961	1.127
	0.27	0.61	(0.75)
1.10	1.099	0.961	1.030
	0.07	0.61	(0.65)

Table 14
Ratio of detector efficiencies for the $C8/F$ experiment for the Cadmium sleeve of 5.0 cm length in the position in the Cadmium covered position.

Cadmium sleeve thickness (mm)	Cadmium covered position ^{239}Np/^{143}Ce Disk/fuel rod σ (%)	Ratio of η_{Np} (277.6 keV)/η_{Ce} (293.4 keV) Disk/fuel rod (1σ (%))	CF_{Cd} σ (%)
0.55	1.203	0.961	1.156
	0.05	(0.61)	(0.71)
1.10	1.071	0.961	1.056
	0.26	(0.61)	(0.68)

Table 15
Calculated factors needed for the spectral indices.

Factor	Condition	Cadmium sleeve thickness (mm)	
		0.55	1.10
Fission rate in ^{238}U	Bare	5.7474×10^{-5}	5.7154×10^{-5}
σ (%)		(0.10)	(0.10)
	Cd covered	4.4258×10^{-5}	4.4175×10^{-5}
		(0.11)	(0.12)
Y_{Ce} (%)	Bare	5.883	5.883
σ (%)		(0.2)	(0.2)
	Cd covered	5.454	5.441
		(0.3)	(0.3)
F_{25}	Bare	0.961	0.961
σ (%)		(0.2)	(0.2)
	Cd covered	0.794	0.782
		(0.2)	(0.3)
ε		0.8914	0.8708
σ (%)		(0.5)	(0.5)

Table 16
Spectral index $^{28}\rho^*$ for the fuel rod.

Length (cm)	T (mm)	$^{28}F_{cor}$	Symmetric position		
		σ (%)	$^{28}R_{Cd}$ σ (%)	$^{28}R_{Cd}$-corr. σ (%)	$^{28}\rho^*$ σ (%)
5.0	0.55	0.9886	1.4231	1.4395	2.276
		(0.1)	(0.1)	(0.2)	(0.5)
5.0	1.10	0.9957	1.4592	1.4655	2.148
		(0.1)	(0.1)	(0.2)	(0.6)

Table 17
Spectral index $^{25}\delta^*$ for the fuel rod.

Length (cm)	T (mm)	$^{25}F_{cor}$	ε	Symmetric position		
		(σ (%))	(σ (%))	$^{25}R_{Cd}$ (σ (%))	$^{25}R_{Cd}$ corr. (σ (%))	$^{25}\delta^*$ (σ (%))
5.0	0.55	1.015	0.8914	7.188	7.082	0.144
		(0.4)	(0.5)	(0.4)	(0.6)	(0.9)
5.0	1.10	1.025	0.8708	7.553	7.369	0.134
		(0.4)	(0.5)	(0.4)	(0.6)	(0.9)

The experimental determination of the spectral indices in the symmetric position basically follows the same steps as already explained previously. Three independent irradiations were found sufficient to get the Cadmium ratios for the ^{239}Np and ^{143}Ce countings, and the spectral index $C8/F$. The factors ε and F_{25} needed for the experimental determination of $^{25}\delta^*$ as given in Eq. (5) were calculated by MCNP5 with the ENDF/B-VII.0 (Oblozinsky and Herman, 2006) nuclear data library. The IPEN/MB-01 reactor was simulated in a 3D model with plenty of details of the experimental configuration and the fission rates of ^{235}U and ^{238}U for the bare and Cadmium covered positions were determined. The ^{143}Ce fission yields come from the CINDER-2 library (Wilson et al., 1995) and are given by: $Y^{25}_{Ce} = 5.9373\%$ for thermal fissions in ^{235}U, $Y^{25}_{Ce} = 5.68627\%$ for epithermal fissions in ^{235}U, and $Y^{28}_{Ce} = 4.5585\%$ for fast fissions in ^{238}U. The final values for ε and F_{25} are given in Table 15.

The constant K used in Eq. (11) was determined using the following operational and physical data: $t_w = 0$, waiting time, $t_I = t_m = 1$ h, irradiation and measurement time, respectively, $g_{Np} = 0.1438$, $g_{Ce} = 0.428$, $\lambda_{Np} = 0.01226$ (h^{-1}), $\lambda_{Ce} = 0.02097$ (h^{-1}), and $\lambda_{U9} = 1.8078$ (h^{-1}). Replacing these constants yields $K = 5.0126$.

The final results for the spectral indices are given in Table 16 for $^{28}\rho^*$, in Table 17 for $^{25}\delta^*$, and in Table 18 for $C8/F$, all for the Cadmium sleeve length of 5.0 cm. $^{28}\rho^*$ and $^{25}\delta^*$ were determined employing Eq. (5) while $C8/F$ employed Eq. (11). R_{Cd}-corr. appearing in Tables 16 and 17 is the Cadmium ratio corrected by the corresponding F_{cor}.

5. Effect of parameter uncertainties on the spectral indices

All parameter uncertainties and how they were derived are described in LEU-COMP-THERM-077 (Dos Santos et al., 2004). Here only the propagation of these uncertainties to the spectral indices is considered. The approach follows basically the same one used in LEU-COMP-THERM-077.

The uncertainty due to the geometrical and material composition data was obtained in the companion HAMMER-TECHNION/CITATION codes. HAMMER-TECHNION (Barhen et al., 1978) is used for the few-group cross-section generation and CITATION (Fowler et al., 1971) (a 3-D deterministic diffusion theory code) is used for the neutron diffusion within the reactor core. The model included all details of the fuel region, control rods, reflector, etc.

Table 18
Spectral index $C8/F$ for the fuel rod.

Length (cm)	T (mm)	Symmetric positions					
		Bare			Cadmium covered		
		CF_{Bare} (σ (%))	$^{239}Np/^{143}Ce$ (σ (%))	$C8/F$ (σ (%))	CF_{Cd} (σ (%))	$^{239}Np/^{143}Ce$ (σ (%))	$C8/F$ (σ (%))
5.0	0.55	1.127 (0.75)	1.295 (0.32)	0.312 (1.04)	1.156 (0.71)	6.543 (0.34)	1.422 (1.05)
5.0	1.10	1.030 (0.65)	1.194 (0.11)	0.314 (0.93)	1.056 (0.68)	6.174 0.02	1.465 (0.97)

Table 19
CITATION calculations of the geometrical and material composition uncertainties for 20 °C.

Parameter	Parameter value ± 1σ	$\Delta^{28}\rho^*$		$\Delta^{28}\rho^*$	$\Delta^{25}\delta^*$		$\Delta^{25}\delta^*$
		+1σ	−1σ	Uncertainty	+1σ	−1σ	Uncertainty
1. ^{235}U enrichment (%)	4.3486 ± 0.0021	−1.55E−03	1.27E−03	1.55E−03	−3.49E−05	2.92E−05	3.49E−05
2 UO_2 density (g/cm^3)	10.1771 ± 0.1018	−7.69E−04	7.64E−04	7.69E−04	−7.62E−04	7.64E−04	7.64E−04
3. UO_2 pellet diameter (mm)	8.4894 ± 0.00475	9.21E−04	−1.22E−03	1.22E−03	5.47E−05	−6.35E−05	6.35E−05
4. Cladding outer diameter (mm)	9.8074 ± 0.0169	−8.01E−04	−3.93E−04	8.01E−04	−1.15E−05	−1.12E−05	1.15E−05
5. Cladding inner diameter (mm)	8.5746 ± 0.0243	8.63E−05	−2.67E−04	2.67E−04	−7.06E−06	−6.54E−06	7.06E−06
6. Pitch (mm)	15.000 ± 0.392	1.84E−03	−1.42E−03	1.84E−03	2.38E−04	−2.41E−04	2.41E−04
7. Active core height (cm)	54.84 ± 0.3544	8.50E−03	−1.08E−02	1.08E−02	1.22E−04	−1.28E−04	1.28E−04
8. Cladding density (g/cm^3)	7.9207 ± 0.0005	0	0	0	0	0	0
9. ^{55}Mn in cladding SS (wt.%)	1.6867 ± 0.11015	0	0	0	0	0	0
10. Cladding composition	Ni = 10.0433 ± 0.125 Cr = 18.34 ± 0.2163 Co = 0.215 ± 0.00707 Mo = 0.17 ± 0.01414	0	0	0	0	0	0
11. ^{234}U (wt.%)	0.034 ± 0.000034	0	0	0	0	0	0
12. UO_2 stoichiometric factor (%)	88.125 ± 0.023	0	0	0	0	0	0
13. Water density (g/cm^3)	0.99820 ± 0.00002[b]	0	0	0	0	0	0
14. Bottom alumina height (mm)	90.28 ± 0.09	0	0	0	0	0	0
15. Control rod density	10.007 ± 0.004	0	0	0	0	0	0
16. Control rod composition	Ag = 0.7934 ± 0.0015 In = 0.1496 ± 0.0014 Cd = 0.0483 ± 0.001	0	0	0	0	0	0
Total[a]	–	–	–	1.12E−02	–	–	8.15E−04

[a] Total uncertainty is equal to $\sqrt{\sum(\Delta^{28}\rho^*)^2}$ or $\sqrt{\sum(\Delta^{25}\delta^*)^2}$.
[b] R.C. Weast (Ed.), 1989. Handbook of Chemistry and Physics, 70th ed. CRC Press. ISBN-O-8493-0470-9.

The convergence criterion used was 1.0E−06. Since the uncertainties in the majority of cases are rather small, the use of a Monte Carlo approach has been discarded because it would require a very large number of neutron histories in order to reduce the standard deviation to a level smaller than the uncertainty itself. The approach adopted based on the deterministic code has been found to be adequate. All parameters and the corresponding uncertainties are at 20 °C. The uncertainties considered are those arising from the ^{235}U enrichment, UO_2 density, UO_2 pellet diameter, cladding outer and inner diameters, pitch, active core height, cladding density and composition, ^{234}U content, UO_2 stoichiometric factor, water density, bottom alumina height, control rod density, and control rod composition. The effect of the fuel impurities on the reactivity was estimated to be of the order of 1 pcm, which is negligible for the analysis considered here. The effect of the water impurities is also small (<1 pcm). Neither will be considered further in the analyses.

Results for the CITATION calculations for the Cadmium sleeve of 1.1 mm thickness and 5.0 cm length are shown in Tables 19 and 20. The $1-\sigma$ value for parameter 1 is the standard uncertainty divided by $\sqrt{8}$ where 8 is the number of fuel batches. The $1-\sigma$ value for parameters 2, 3 and 7 is the standard uncertainty divided by $\sqrt{680}$ where 680 is the number of fuel rods, while those of parameters 4 and 5 were divided by $\sqrt{162}$, where 162 is the number of measurements of the inner and outer diameters of the cladding.

Combining the geometric and material uncertainties from Tables 19 and 20 and the experimental uncertainties for $^{28}\rho^*$, $^{25}\delta^*$, $(C8/F)_{ept}$, and $C8/F$ given in Tables 15–17, respectively, the total uncertainties in these parameters (σ_t) can be obtained as:

$$\sigma_t(^{28}\rho^*) = \sqrt{(1.29\times10^{-2})^2 + (1.12\times10^{-2}))^2} \cong 1.71\times10^{-2} \tag{15}$$

$$\sigma_t(^{25}\delta^*) = \sqrt{(1.22\times10^{-3})^2 + (8.15\times10^{-4})^2} \cong 1.47\times10^{-3} \tag{16}$$

$$\sigma_t((C8/F)_{ept.}) = \sqrt{(1.45\times10^{-2})^2 + ((1.85\times10^{-3}))^2} \cong 1.46\times10^{-2} \tag{17}$$

$$\sigma_t((C8/F)) = \sqrt{(2.99\times10^{-3})^2 + (1.29\times10^{-3})^2} \cong 3.26\times10^{-3} \tag{18}$$

Since the cases are very similar the results reported in Tables 19 and 20 can be extended to the Cadmium sleeve thickness of 5.5 mm.

Table 21 summarizes the values of spectral indices. Since the total uncertainty is small and well understood, the proposed experiment is acceptable as a benchmark experiment.

Table 20
CITATION calculations of the geometrical and material composition uncertainties for 20 °C.

Parameter	Parameter value ± 1σ	$\Delta(C8/F)_{ept}$[a]		$\Delta(C8/F)_{ept}$	$\Delta C8/F$		$\Delta C8/F$
		+1σ	−1σ	Uncertainty	+1σ	−1σ	Uncertainty
1. ^{235}U enrichment (%)	4.3486 ± 0.0021	2.20E−04	−2.03E−04	2.20E−04	7.86E−05	−7.05E−05	7.86E−05
2 UO_2 density (g/cm^3)	10.1771 ± 0.1018	−4.61E−04	4.66E−04	4.66E−04	8.95E−04	−9.05E−04	9.05E−04
3.UO_2 pellet diameter (mm)	8.4894 ± 0.00475	2.92E−04	−3.03E−04	3.03E−04	−2.04E−05	2.79E−05	2.79E−05
4. Cladding outer diameter (mm)	9.8074 ± 0.0169	2.92E−04	6.71E−04	6.71E−04	1.69E−04	4.68E−04	4.68E−04
5. Cladding inner diameter (mm)	8.5746 ± 0.0243	3.37E−04	1.41E−03	1.41E−03	4.68E−04	4.68E−04	4.68E−04
6. Pitch (mm)	15.000 ± 0.392	7.31E−04	−7.56E−04	7.56E−04	−2.53E−04	2.61E−04	2.6E−04
7. Active core height (cm)	54.84 ± 0.3544	2.18E−04	−2.57E−04	2.57E−04	−5.81E−04	5.85E−04	5.85E−04
8. Cladding density (g/cm^3)	7.9207 ± 0.0005	0	0	0	0	0	0
9. ^{55}Mn in cladding SS(wt.%)	1.6867 ± 0.11015	0	0	0	0	0	0
10. Cladding composition	Ni = 10.0433 ± 0.125 Cr = 18.34 ± 0.2163 Co = 0.215 ± 0.00707 Mo = 0.17 ± 0.01414	0	0	0	0	0	0
11. ^{234}U (wt.%)	0.034 ± 0.000034	0	0	0	0	0	0
12. UO_2 stoichiometric factor (%)	88.125 ± 0.023	0	0	0	0	0	0
13. Water density (g/cm^3)	0.99820 ± 0.00002[b]	0	0	0	0	0	0
14. Bottom alumina height (mm)	90.28 ± 0.09	0	0	0	0	0	0
15. Control rod density(g/cm^3)	10.007 ± 0.004	0	0	0	0	0	0
16. Control rod composition	Ag = 0.7934 ± 0.0015 In = 0.1496 ± 0.0014 Cd = 0.0483 ± 0.001	0	0	0	0	0	0
Total[c]	–	–	–	1.85E−03	–	–	1.29E−03

[a] The subscript ept. means epithermal or Cadmium covered.
[b] Weast, R.C. (Ed.), 1989. Handbook of Chemistry and Physics, 70th ed. CRC Press. ISBN-O-8493-0470-9.
[c] Total uncertainty is equal to $\sqrt{\sum(\Delta(C8/F)_{ept})^2}$ or $\sqrt{\sum(\Delta(C8/F))^2}$.

Table 21
Benchmark model spectral indices.

Length (cm)	Thickness (mm)	Symmetric positions			
		$^{28}\rho^*$ σ (%)	$^{25}\delta^*$ (σ (%))	Bare $C8/F$ (σ (%))	Cd covered $C8/F$ (σ (%))
5.0	0.55	2.276 (0.80)	0.144 (1.10)	0.312 (1.13)	1.422 (0.98)
5.0	1.10	2.148 (0.90)	0.134 (1.30)	0.314 (1.00)	1.465 (0.98)

6. Theoretical analysis of spectral index calculations

The theoretical analysis of the spectral index experiments realized at the IPEN/MB-01 research reactor facility was performed employing the Monte Carlo MCNP-5 (X-5 Monte Carlo Team, 2003). The nuclear data libraries used for this analysis were ENDF/B-VII.0 (Oblozinsky and Herman, 2006), ENDF/B-VI.8 (ENDF/B-VI Summary Documentation, 2000), JEF3.1 (NEA Data Bank, 2006), and JENDL3.3 (Shibata et al., 2002).

The quantities to be calculated are expressed mathematically as:

$$RR_x = \int \cdots \int \Sigma_x(r, E')\phi(r, \Omega', E')dr d\Omega' dE', \tag{19}$$

where RR_x represents the reaction rate of type x (either neutron capture in ^{238}U or neutron fissions in ^{235}U or ^{238}U), E is the neutron energy, $\Sigma_x(r, E)$ is the macroscopic cross section for reaction x of the fuel region at position r and neutron energy E, Ω is the neutron energy direction, $\phi(r, \Omega, E)$ is the neutron flux at position r, and direction Ω and energy E. The volume integral is performed in a cylindrical region whose radius is the pellet radius and its height is equal to 1.0 cm. The axial position of the center of the cylinder is equal to 10.0 cm for the bare case and 35.0 cm for the Cadmium covered region, both distances from the bottom of the active length of the fuel rod. The Cadmium ratio (R_{Cd}) is calculated as the ratio between the reaction rates in the bare position to that in the Cadmium covered position. The spectral indices (either $^{28}\rho^*$ or $^{25}\delta^*$) are subsequently calculated as:

$$SI = \frac{1}{R_{Cd} - 1}. \tag{20}$$

($C8/F$) in the bare and Cadmium covered positions are calculated accordingly from the ratio of ^{238}U captures and total fissions.

The benchmark model is shown in Figs. 3 and 4. All geometric and material data for the regions of the IPEN/MB-01 reactor is reported in Dos Santos et al. (2012). Only the final results are reported in this work.

The calculations simulated all regions that comprise the benchmark model of the IPEN/MB-01 reactor. The MCNP-5 runs simulated 24×10^9 neutron histories. The critical control bank positions were considered accordingly for the two types of the Cadmium sleeve considered in this work.

The theory/experiment comparison of the spectral indices calculated by MCNP-5 with ENDF/B-VII.0, ENDF/B-VI.8, JENDL3.3, JEF3.1 libraries for a Cadmium sleeve length of 5.0 cm and thicknesses 0.55 mm and 1.1 mm are shown respectively in Tables 22 and 23. All cases except the last one of Table 22 utilizes the function S(α, β) from ENDF/B-III (Koppel and Houston, 1978) (lwtr.01 of MCNP-5 library). The last case utilizes S(α, β) from ENDF/B-VII.0 as well as the remainder of the nuclear data are also from this library. Tables 22 and 23 also show in the last column k_{eff} for the several libraries and for the two Cadmium sleeve thickness

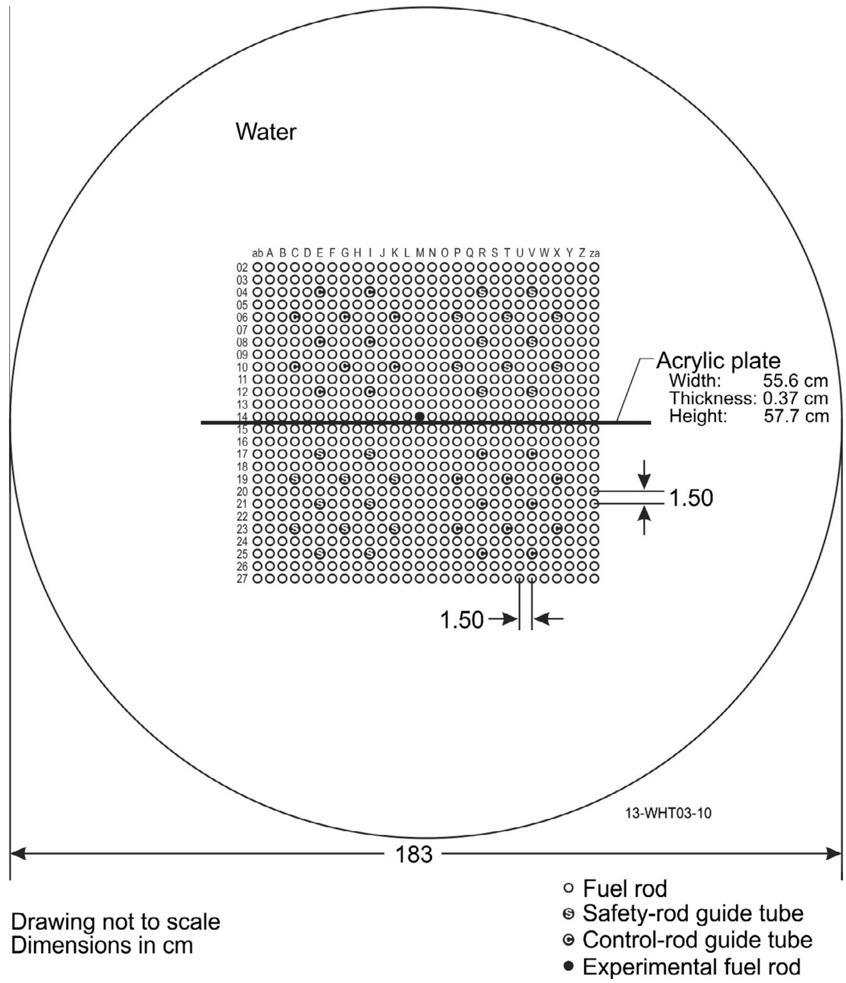

Fig. 3. Radial representation (midway plane) of the IPEN/MB-01 core.

analyzed in this work. The uncertainty assigned to k_{eff} is 60 pcm, good part of that due to the material and geometric data of the IPEN/MB-01 reactor. This uncertainty arose from the several critical experiments and analysis of the IPEN/MB-01 reactor published at the ICSBEP handbook (Briggs, 2012). Because thermocouples and control and instrumentation tubes are not included in the calculation model, the total of their measured reactivity effect (−33.5 pcm) is included as a bias to k_{eff} of the benchmark model (−12.5 pcm for omitting thermocouples and −21 pcm for omitting neutron detectors). LEU.COMP.THERM.077 describes all the reasoning behind the values of these biases. Therefore, the value of k_{eff} to be considered for theory/experiment comparison is 1.00033 ± 0.00060.

The theory/experiment comparison reveals, that independently of the nuclear data library employed in the analysis, an excellent agreement for the spectral index $^{28}\rho^*$; aspect never found before in several other comparisons (Courcelle et al., 2006; Dos Santos et al., 2004). The approach adopted in the IPEN/MB-01 experiment for the experimental determination of the spectral index $^{28}\rho^*$ shows that the elimination of all calculated correction factors freed the final result of possible bias. Consequently the theory/experiment comparison was more reliable and accurate. Surprising result was found for ENDF/B-VI.8 which shows excellent agreement for $^{28}\rho^*$. The procedure adopted in ENDF/B-VII.0 to reduce the epithermal cross sections of ^{238}U by around 0.4% and the corresponding thermal cross sections of this nuclide by nearly 1.5% is completely supported by the IPEN/MB-01 experiments. The results for $^{28}\rho^*$, $(C8/F)_{ept}$ and k_{eff} support these reductions in the values of the aforementioned cross sections. The set of benchmark values reported in Tables 22 and 23 is very appropriate to test the cross sections of thermal systems with slightly enriched uranium. Since the spectral indices are ratio of reaction rates, any systematic reduction or increase in the thermal and epithermal reaction rates will yield the same spectral index.

However k_{eff} of the system will not remain the same in this case. This is clear for the $^{28}\rho^*$ case of ENDF/B-VI.8. The agreement of $^{28}\rho^*$ to the benchmark value is excellent but its k_{eff} is underpredicted by around 350 pcm which is consistent to the other benchmark analysis (Courcelle et al., 2006; Van der Marck and Hogenbirk, 2003). This aspect does not happen when ENDF/B-VII.0 is employed since the nuclear data of ^{238}U was changed to reflect the physics of the neutron interaction more precisely. The k_{eff} results of ENDF/B_VII.0 of this work are consistent with other benchmark analysis (Van Der Marck, 2006). The theory/experiment comparison of $^{25}\delta^*$ and $(C8/F)$ shows that these spectral indices are in general slightly overpredicted. At first sight it could be suggested that the thermal fission cross section of ^{235}U could be underestimated. However, when the function $S(\alpha,\beta)$ is changed to that of ENDF/B-VII.0 the $(C-E)/E$ values of $^{25}\delta^*$ and $(C8/F)$ improves considerably but still a slight overprediction is noticed. Therefore, there is an indication that the thermal spectra are strongly affected by the $S(\alpha,\beta)$ function and consequently all thermal reactions. Whether or not the fission cross section of ^{235}U is underestimated is very difficult to say because the analysis has been made considering just 1σ range

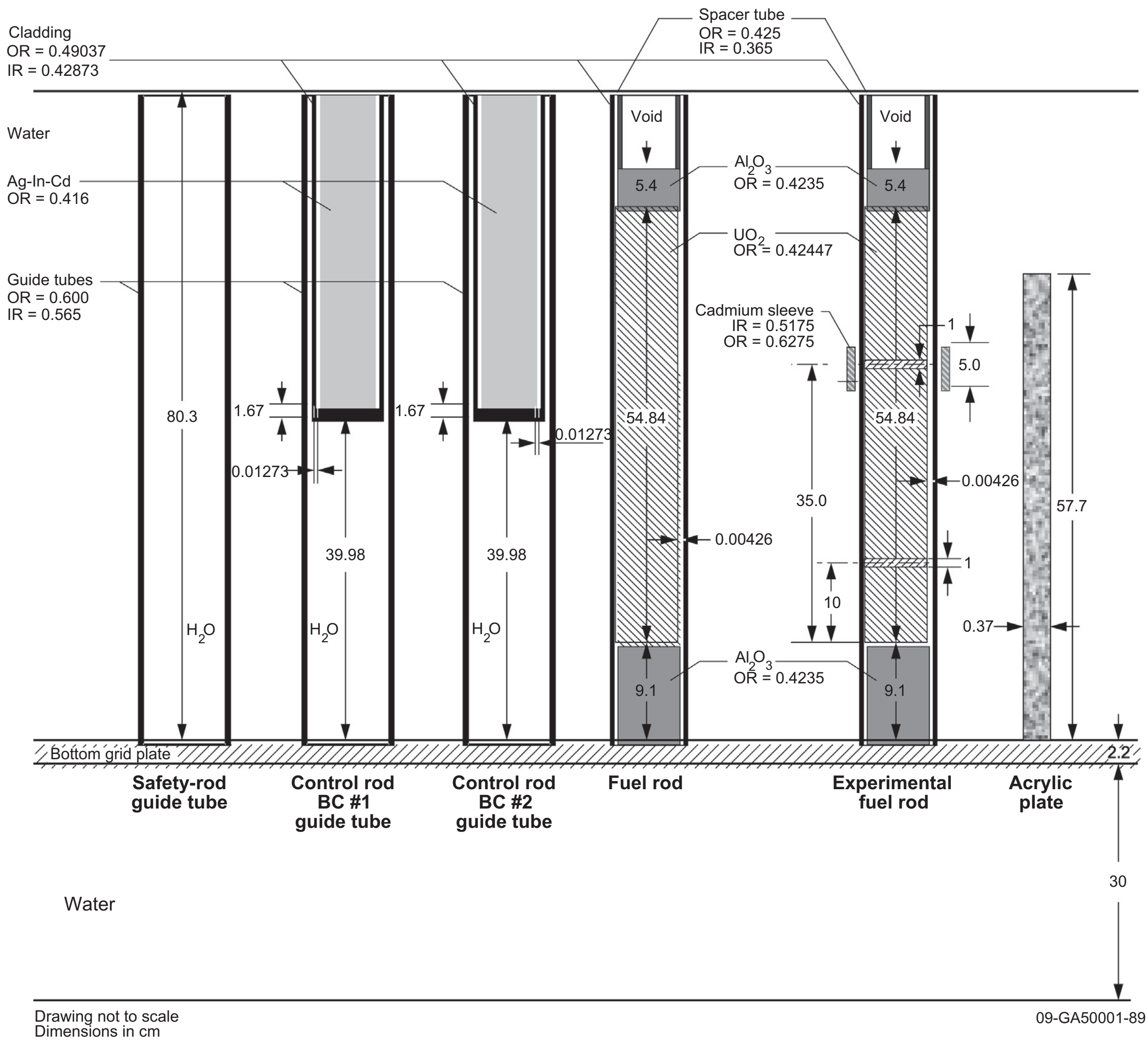

Fig. 4. Representation of the: fuel rod, the control rods inside their guide tubes, the safety-rod guide tube, the experimental fuel rod, and the acrylic plate in the benchmark model.

Table 22
Theory/experiment comparison of the spectral indices for the Cadmium sleeve length of 5.0 cm and thickness 0.55 mm.

Library	$(C-E)/E$ (%)				k_{eff}
	$^{28}\rho^*$ (σ (%))	$^{25}\delta^*$ (σ (%))	$C8/F$ (σ (%))	$(C8/F)_{ept}$ (σ (%))	
ENDF/B-VII.0	−0.36 (0.58)	2.34 (0.58)	1.51 (0.58)	−0.27 (0.53)	1.00085 ± 0.00001
JENDL3.3	−1.18 (0.58)	1.89 (0.58)	2.61 (0.58)	0.66 (0.53)	0.99949 ± 0.00001
JEF3.1	−0.98 (0.58)	1.83 (0.58)	1.73 (0.58)	−0.22 (0.53)	1.00058 ± 0.00001
ENDF/B-VI.8	−0.07 (1.16)	2.08 (1.16)	2.36 (1.17)	0.38 (1.07)	0.99653 ± 0.00001
S(α, β) B-VII.0	−0.54 (1.16)	1.41 (1.16)	1.22 (1.17)	−0.18 (1.07)	1.00161 ± 0.00001

Table 23
Theory/experiment comparison of the spectral indices for the Cadmium sleeve length of 5.0 mm and thickness 1.1 mm.

Library	$(C-E)/E$ (%)				k_{eff}
	$^{28}\rho^*$ (σ (%))	$^{25}\delta^*$ (σ (%))	$C8/F$ (σ (%))	$(C8/F)_{ept}$ (σ (%))	
ENDF/B-VII.0	−0.11 (0.60)	1.92 (0.51)	0.95 (0.50)	0.29 (0.49)	1.00093 ± 0.00001
JENDL3.3	−1.41 (0.58)	1.47 (0.58)	2.01 (0.58)	1.13 (0.53)	0.99957 ± 0.00001
JEF3.1	−1.06 (0.60)	1.37 (0.56)	1.19 (0.50)	0.83 (0.49)	1.00066 ± 0.00001

of the experimental uncertainty. If 2σ range of the experimental uncertainty is considered all spectral index comparison come into excellent agreement.

The effect of the function S(α, β) of ENDF/B-VII.0 on k_{eff} is also noticeable in Table 22 since it increases. It might indicate that the thermal fissions in ^{235}U are also increasing relatively to its neutron capture events. The k_{eff} is shown for consistency and with exception to the ENDF/B/VI.8 case; all other libraries show excellent agreement.

7. Conclusions

The experiment performed at the IPEN/MB-01 reactor was successfully designed, executed and evaluated. The experiment and the corresponding results are well documented and with uncertainties small enough and well understood suitable for a benchmark problem. The complete evaluation reported in the IRPhE handbook has shown to be very useful to test and verify the current and new versions of the nuclear data libraries for thermal reactor application. Specifically for the $^{28}\rho^{*}$ case, the experimental results did not require any sort of calculated correction factors which gave to the IPEN/MB-01 experiment an excellent quality and free of possible bias. The theory/experiment comparisons performed in this work suggest that the determination of this spectral index in former experiments might be affect by possible bias due to the introduction of the calculated correction factors. From the overall analysis of this work, it was concluded that the experiments performed at the IPEN/MB-01 reactor supports the changes in the ^{238}U nuclear data incorporated in ENDF/B-VII.0 and in the other libraries studied in this work. The theory/experiment comparison of $^{25}\delta^{*}$ and $(C8/F)$ show that these spectral indices are in general slightly overpredicted. At first sight it could be suggested that the thermal fission cross section of ^{235}U could be underestimated. However, when the function $S(\alpha,\beta)$ is changed to that of ENDF/B-VII.0 the $(C-E)/E$ of $^{25}\delta^{*}$ and $(C8/F)$ improves considerably but still a slight overprediction is noticed. Therefore, there is an indication that the thermal spectra are strongly affected by this function and consequently all thermal reactions. Whether or not the fission cross section of ^{235}U is underestimated is very difficult to say. The effect of the function $S(\alpha,\beta)$ of ENDF/B-VII.0 on k_{eff} is also noticeable in Table 22. Finally, as already seen in several other studies, ENDF/B-VII.0 is making very good progress for utilization in thermal reactor applications.

References

Barhen, J., Rhotenstein, W., Taviv, E., 1978. The Hammer Code System. Technion-Israel Institute of Technology, Haifa, Israel. EPRI-NP-565.

Bevington, P.R., 1969. Data Reduction and Error Analysis for the Physical Sciences. McGraw Hill.

Bitelli, U.d'U., 2001. Medida de Parâmetros Integrais no Reator IPEN/MB-01. Tese de Doutorado – IPEN.

Bitelli, U.d'U., Dos Santos, A., 2002. The Spectral Indices of the IPEN/MB-01 Reactor: Measurements and Calculations. PHYSOR 2002 International Topical Advances in Reactor Physics and Mathematics and Computation, Seoul, Korea, October 7–10.

Briggs, J.B. (Ed.), 2012. International Handbook of Evaluated Criticality Safety Benchmark Project. NEA/NSC/DOC (95)03, Nuclear Energy Agency, OECD, Paris, France.

Courcelle, A. et al., 2006. Nuclear Data for Improved LEU-LWR Reactivity Predictions. OECD Nuclear Energy Agency, NEA/WPEC-22.

Cross Section Evaluation Working Group Benchmark Specification, 1974. ENDF-202/BNL-19302. Brookhaven National Laboratory.

Dos Santos, A. et al., 2012. IPEN (MB01)-LWR-CRIT-SPEC-REAC-COEF-KIN-RRATE-POWDIS-001: Reactor Physics Experiments in the IPEN/MB-01 Research Reactor Facility. International Handbook of Evaluated Reactor Physics Benchmark Experiments. Nuclear Energy Agency (NEA DATA BANK), Paris, pp. 1–142.

Dos Santos, A., Fanaro, L.C.C.B., Yamaguchi, M., Jerez, R., Andrade e Silva, G.S., Siqueira, P.T.D., Abe, A.Y., Fuga, R., 2004. Critical loading configurations of the IPEN/MB-01 reactor, LEU-COMP-THERM-077. In: Briggs, J. Blair (Ed.), International Handbook of Evaluated Criticality Safety Benchmark Experiments, NEA/NSC/DOC (95)03/I, Paris, September.

ENDF/B-VI Summary Documentation, 2000. In: Rose, P.F. (Ed.), BNL-NCS-17451 (ENDF-201), 4th ed. (ENDF/B-VI). National Nuclear Data Center, Brookhaven National Laboratory, Release-8.

Fowler, T.B., Vondy, D.R., Cunninghan, G.W., 1971. Nuclear Reactor Core Analysis Code: CITATION. ORNL-2496, Version 2.

Hardy Jr., J., 1983. ENDF/B Data Testing results for Thermal Reactor Benchmark. Thermal Reactor Benchmark Calculation, Techniques, Results and Applications, BNO-NP-1983.

Koppel, J.U., Houston, D.H., 1978. Reference Manual for ENDF Thermal Neutron Scattering Data. Report General Atomics: GA-8774 (ENDF-269).

Nakajima, K., Akai, M., Suzaki, T., 1994a. Measurements of the modified conversion ratio by gamma-ray spectrometry of fuel rods for water-moderated UQ2 cores. Nucl. Sci. Eng. 116, 138–146.

Nakajima, K., Akai, M., Yamamoto, T., Suzaki, T., 1994b. Measurements and analyses of the ratio of ^{238}U captures to ^{235}U fission in low-enriched UO_2 tight lattices. J. Nucl. Sci. Technol. 31, 1160–1170.

NEA Data Bank, 2006. JEFF Report 21: The JEFF-3.1 Nuclear Data Library. <http://www.nea.fr/html/dbdata/nds_jefreports/jeffreport-21/index.html>.

Oblozinsky, O., Herman, M., 2006. Special Issue on Evaluated Nuclear Data File ENDF/B-VII.0. Nuclear Data Sheets 107(12).

OriginLab Corporation, Data Analyses and Technical Graphics, ORIGIN-6.1.

Rahman, M., Mandal, M.A.W., Alam, B., Takano, H., 2004. Validation study of the cell code WIMS-D and a 69 group library based on JENDL-3.2. Ann. Nucl. Energy 31, 1357–1383.

Reus, U., Westmeier, W., 1983. Atomic Data and Nuclear Data Tables. Academic Press, Marburg.

Sher, R., Fiarman, S., 1976. Studies of Thermal Reactor Benchmark Data Interpretation: Experimental Corrections. Stanfordy University, Stanford.

Shibata, K. et al., 2002. Japanese evaluated nuclear data library Version 3 Revision-3: JENDL3.3. J. Nucl. Sci. Technol. 39(11), 1125–1136.

Smith, D.L., 1991. Probability, statistics, and data uncertainties. In: Nuclear Science and Technology. Series: Neutron Physics and Nuclear Data in Science and Technology. Published by Nuclear American Society.

Van der Marck, S.C., Hogenbirk, A., 2003. Criticality Results for Many Benchmark Cases: The Releases JEFF-3.0, ENDF/B-VI.8, JENDL-3.3, ENDF-B/VII-prelim, and BRC, JEFDOC 974.

Van der Marck, S.C., 2006. Benchmarking ENDF/B-VII.0. Nuclear Data Sheets, 107(12).

Wilson, W.B. et al., 1995. Recent development of CINDER'90 transmutation code and data library for actinides transmutation studies. In: GLOBAL'95 International Conference, Versailles, France.

X-5 Monte Carlo Team, 2003. MCNP – A General Monte Carlo N-Particle Transport Code, Version 5. LA-UR-03-1987.

Yudkevich, M.S., Becker, R., Gado, J., Kereszturi, A., Pshenin, V., 1994. Theoretical Investigations of the Physica1 Properties of WWER-TYPE Uranium–Water Lattices. Final Report of Temporary International Collective, vol. 2. Akadémiai Kiad6, Budapest.